Manufacturing of ultra-fine particle CFA-A380 aluminium matrix composites with improved mechanical properties by improved ring milling and oscillating micro-grid mixing

Georgios Kaisarlis [(1)], Georgios Vasiliou [(1)], Vasileios Spitas [(1)], Vassilis Inglezakis [(2)], Grigorios Itskos [(3)], Christos Spitas [(2,c)]

[(1)] School of Mechanical Engineering, National Technical University of Athens

[(2)] School of Engineering, Nazarbayev University

[(3)] College of Engineering, Purdue University

[(c)] Corresponding author: cspitas@gmail.com

Keywords

A380 aluminium alloy; ultra-fine Coal Fly Ash (CFA); metal matrix composites; high energy ring-milling; mechanical testing

Abstract

An experimental study is presented of ultra-fine Coal Fly Ash (CFA) aluminium matrix composites produced by successive high power ring milling of CFA, oscillating micro-grid mixing of the CFA-aluminium melt, gravity casting and rapid cooling. Samples corresponding to different CFA concentrations and particle size distributions (1 μm average, or less) are produced and subjected to microstructural and mechanical characterisation, including tensile, compressive, impact, hardness and wear testing. While the usual trade-off between increased strength and hardness and reduced ductility and toughness is observed, the obtained ultra-fine particle composites are confirmed to have overall improved mechanical properties compared to composites with larger size particles previously produced by ball milling.

1. Introduction

Metal matrix composites (MMCs) reinforced with particle size distributions in the tens of microns to the sub-micron range are known to provide an increase in strength, stiffness, and wear resistance compared to the matrix alloy [1-3], combined with relative ease of manufacture and low cost compared to other composite technologies, e.g. fibre composites.

Coal fly ash (CFA) in particular is a suitable such candidate for micro-/ nano-reinforcement since it is an abundant and cheap by-product of coal burning in thermal power-plants, which is usually disposed of in the form of a chemically inert waste material. CFA can be collected from many points of the exhaust gases route in a thermal power plant, but those used as reinforcements in MMCs are usually collected from the electrostatic precipitator.

Following the original publications by Rohatgi [4-5], many researchers have been experimenting with CFA as reinforcement in non-ferrous MMCs such as aluminium and magnesium; recently, suggestions have been made that improvement in hardness, tensile properties, compressive properties and wear resistance can be obtained with increasing the

content of CFA in the MMCs up to 15 wt% [6-12]. They also suggest that the finer the size of the CFA particles and the more uniform their distribution in the melt the higher the improvement in mechanical properties [13].

Al- based MMCs in particular, mostly produced by stir casting to ensure sufficient interface reaction time between the liquid aluminium alloy and the particles of the reinforcing material (Asthana, 1998), have received considerable attention in the past few decades, in particular with regard to obtaining superior strength, wear resistance and hardness [14-15]. Wu et al. [16] studied the mechanical properties of Al-12% Si alloy and found that addition of 3-7 vol% of short aluminosilicate fibres resulted in a considerable increase in ultimate tensile strength, as later established in Chawla [17]. Ünlü [18] and Kumar et al. [19] confirmed similar benefits when adding Al2O3 to Al6061 alloys and SiC to Al7075 alloys. Wahab, et al. [20] had long confirmed similar effects when adding Al nitride to an Al matrix. Reinforcement of Al2024 alloy with SiC and graphite particles also showed an increase in ultimate tensile strength, compressive strength, yield strength and hardness [21] although this observation was contradicted in a study by Hong (2003). Furthermore, Al will react with other alloying elements, e.g. Mg, to form bimetallic compounds, with important implications for its casting process [22-23].

CFA has received considerable attention as a reinforcing material for light metal alloys, such as aluminium and magnesium, and experiments on Al-alloy/ SiC/ CFA composites showed that increasing the volume fraction of SiC increased wear resistance and hardness, with the composites produced by powder metallurgy manifesting a maximum tensile strength at 10 vol%, while higher fractions produced lower values [24]. CFA-reinforced Al-4.5% Cu alloys have been shown to exhibit the same trends [25]. The extent to which CFA particle size affects the observed reinforcing mechanisms has also received attention. A study on CFA reinforced A356 alloy with different size ranges of 53-106μm and 0.5-400μm showed the expected increase in hardness and stress at 0.2% elongation, as well as an increase in the apparent stiffness [26]. According to the same study, the narrower particle size range led to superior mechanical properties, although with the wide particle size distributions used, it cannot be readily clear if the main factor affecting the mechanical properties in this case was the mean value or the standard deviation of the size distribution, or if there were perhaps very different contributions from the various particle sizes. The positive effect of using fine CFA particles on the mechanical performance of such composites has been also confirmed, in case of wear resistance, by Itskos [27]. Rothagi et al. [28] studied the effect of adding 5-15 wt% CFA cenospheres in die-cast magnesium alloy AZ91D. As a result, tensile strength and hardness increased, while the voids introduced by the unfilled cenospheres let to a decrease in the density and the elastic modulus, as measured by a pulse-echo method.

Anilkumar et al. [12] studied more comprehensively the effect of CFA percent weight (wt%) content and particle size on ultimate tensile strength, hardness and elongation, considering a 0-20 wt% range and three size ranges 4-25 μm, 45-50 μm and 75-100 μm. A clear trend emerged that the finer particle sizes amplified the positive effects on strength and hardness and reduced the negative effects on ductility. Importantly, this trend suggests that even higher benefits may be obtained with finer particle sizes. Also, wt% larger than 15% in that study led to a slight deterioration of the ultimate tensile stress, indicating an optimum at around that CFA content, regardless of particle size.

Murthy et al. [13] focused particularly on the CFA powder obtained by ball milling and showed that particularly fine powder sizes are attainable, however requiring milling times of the order

of 30 h, making this an impractical process outside of the research laboratory, due to its low productivity. The measured mechanical properties of AA2024 alloy fly-ash composite confirmed the trends from the preceding studies.

While MMCs, including the CFA composites, have been shown to almost consistently afford superior strength and hardness compared to their matrix alloys alone, they have been also shown to lower ductility and toughness [29]. Although ageing can be employed to further improve strength and hardness, while also marginally improving the ductility compared to the unaged composite, the compromise in the mechanical properties remains an issue that is not commonly addressed in studies of CFA-aluminium, including the studies referenced above.

It can be concluded from what is known so far that in order to obtain MMCs with superior mechanical properties, their fabrication method should comprise high-energy milling to pulverise the fly-ash to ultra-fine-sized particles and efficient de-agglomeration of the nanoparticles and uniform dispersion in the melt.

However, due to limitations in the ubiquitous planetary ball milling process, all reported studies to-date have used CFA particles milled to average sizes of over 4 μm, with milling times as much as 30 hrs. The supposed benefits from milling the CFA reinforcement to finer sizes have not been so far confirmed in an experimental study.
Furthermore, there are very few studies that attempt a simultaneous characterisation of strength (tensile, compressive, hardness) and ductility (elongation, toughness) of CFA-aluminium composites and none that have done this for very small particle sizes.

To address this gap, the present work utilises an improved ring mill design (based on Spitas, 1999) for ultra-fine powder milling to produce a sharp particle size distribution with average of 1 μm in 120 min, as opposed to over 4μm average obtained by planetary ball milling in 30 hrs [12]. This ultra-fine powder is finely dispersed and mixed in molten CFA-A380 aluminium alloy using an oscillating micro-grid and subsequently gravity-cast and quenched in metal moulds. Having thus ensured an ultra-fine particle size distribution and uniform mixing of the CFA –alloy composite melt, an experimental parametric investigation is conducted of the microstructure and mechanical properties of cast CFA A380 aluminium alloy samples with wt% CFA content varying between 0 and 10%, which is the range that has been indicated as giving the best overall improvement in mechanical properties of CFA MMCs [12].

2. High energy ring-mill pulverization of CFA to ultra-fine particle sizes

The apparatus used in this study is a specially redesigned ring mill based on an original high energy ring mill pulveriser developed and validated at the Machine Design Laboratory of the NTUA (Fig. 1a), comprised of a cylindrical cavity (1), a plurality of parallel rods (2) and a selectable number of annular metallic rings (6). The particles are ground in the space formed between the inner surface of the cylindrical cavity and the annular metal rings (interface 1-6). Consequently, particles are pulverised under the simultaneous effect of normal (compaction) and shear forces. The system has exhibited exceptional results in producing fine powders below 10μm in other applications [29-30].

For the requirements of the present study finer particle sizes had to be obtained, necessitating larger crushing forces. Given the limitations in rotating speed and overall size of the apparatus, the ring mass had to be increased. Also, the function of the original ring mill design produced

significant friction at interfaces (1-6) and (2-6), which in turn resulted in wear and metallic debris. In the present work the existence of such debris is undesirable, as it would contaminate the CFA. Therefore, a redesign of the ring-mill was necessary in order to eliminate metal to metal sliding and thus prevent wear and the subsequent creation of metal debris (Fig. 1b).

The simple ring-rod assembly was substituted by an assembly of a sealed self-aligning spherical bearing (5), having a surface hardened ring (6) mounted on its outer face and connected with the rod (2) via an eccentric hub (4). The bearing and hub are substantially more massive than the original ring, producing a much higher centrifugal force. A wear-free self-adjusting rotating motion of the eccentric (4) relative to the rod (2) is furthermore allowed by means of a plain bearing (3) connecting the two parts. As in the original design, a plurality of these subassemblies 3-4-5-6 are mounted along each rod. The operating principle of the improved ring mill, including the vector equilibrium of the main operating forces, is illustrated in Fig. 1c.

Furthermore, the housing (1) was fitted with cooling channels connected to a cold water supply, resulting in good temperature control and higher efficiency of the milling process. The ring mill is driven by an AC electrical motor able to control rotation speed via the use of an inverter. The redesigned ring-mill used in this study is shown in Fig. 1d.

3. CFA melt mixing and de-agglomeration

A significant challenge in developing CFA MMCs is to ensure that CFA particles are sufficiently dispersed in the metallic melt. CFA particles in storage tend to form agglomerates held together by steric interactions as well as by Van der Waals forces. The very high surface-to-volume ratio makes their disentanglement and dispersion difficult [31].

In order to properly disperse the CFA agglomerates inside the aluminium alloy melt more effectively, a micro-structured oscillating micro-grid melt-mixer is used [32] (Fig. 2a-b). It consists of a stationary stainless-coated hollow cylinder, in which parallel grids mounted on a perforated piston-rod assembly oscillate vertically, thus causing extensional and shear flow of the melt metallic mixture contained in the cylinder as its volume is repeatedly swept by the piston. Details of the design and modelling of the melt-mixer can be found in Kaisarlis [32] and are not iterated here.

4. Fabrication of samples

4.1. CFA pulverisation and characterisation

The CFA used in this study was collected under maximum electricity load from the electrostatic precipitators of the Ekibastuz plant in Astana, Kazakhstan. Prior to its characterisation the CFA batch used in this study was homogenized and dried in oven at 70 °C for 12 h.

The elemental composition of the Ekibastuz CFA was obtained on XRF (PANalytical Axios) and is shown in Table 1. According to data the main elements containing in raw CFA are Al, Si, Fe and Ca, which was expected. Compared to CFA compositions from other sites in Kazakhstan [33] and the rest of the world [34-37], the particular CFA contained a substantially higher amount of iron oxide and a slightly lower content in aluminium oxide.

A representative XRD spectrum of fly ash used in this study is shown in Fig. 3. The XRD pattern was recorded on a SmartLab X-ray diffraction instrument (Cu, K-β filter, 40 kV and 30 mA) with

a diffraction angle of 2θ and a scanning range of 5–100◦ (Rigaku). The results show that the main minerals present are quartz, mullite and magnetite/hematite. The XRD semi-quantitative analysis shows that the content of crystalline mullite and quartz are 67% and 33%, respectively. It should be noted that the amount of magnetite/hematite present in the sample cannot be detected in XRD as is mostly amorphous and thus only crystalline particles of this phase were used for the calculation of the above percentages.

The milled CFA was observed with SEM, revealing a predominantly spherical morphology, containing a small number of oblate spheroidal, ellipsoidal particles and a few seemingly broken particles with sharp edges. In order to disperse the agglomerates, the CFA was diluted in ethanol to form 1.5 vol% suspension and after drying it was examined under a LEICA HC optical microscope. The particle size distribution was measured by processing of the optical image using the accompanying software and is shown in Fig. 4a.

The CFA was dried and placed in the high performance ring mill, which measures ∅160x80 mm (roughly 2 lt in volume). The interior of the mill was filled with dry nitrogen gas at room temperature and ambient pressure. Each batch of fly ash (weighting 100 g) was placed inside the ring mill and was ground continuously at 1400 rpm for 120 min and the pulverised CFA was extracted from it in the end. No regrind was used in the process. A sample of this was examined in the optical microscope, revealing that multiple agglomerates had formed due to van der Waals interactions after exposure of the pulverised CFA to air moisture.

In order to disperse the agglomerates into singular particles, pulverised fly ash was diluted in 98% ethanol and mixed to form a 1.5% vol. suspension. The suspension was then dried and observed under the optical microscope, which confirmed that the pulverisation process managed to produce very fine solitary particles in the order of microns or in the sub-micron range, which can be seen in Fig. 5. The exact particle size distribution can be seen in Fig. 4b and is seen to be exceptionally sharp compared to other results reported in the literature [12-13]. The average size of approx. 1μm, achieved in 2hrs with the high-energy ring mill, is four times smaller than the value obtained by Anilkumar [12] in 30 hrs with a planetary ball mill, confirming that the process proposed in this paper is substantially more effective.

A secondary 'ultra-fine' sample was extracted from a part of the 'fine' pulverised CFA sample in the diluted and suspended form by pressing it slowly through a 0.5 μm membrane filter. Thus two different samples were set aside for the subsequent testing, the 'fine' sample following the particle size distribution of Fig. 4b and the 'ultra-fine' sample almost exclusively comprised of <0.5 μm particles.

4.2. CFA melt mixing and casting

Melt mixing was performed using the melt mixer presented in sections 3 and 4. The pouring temperature was set at 650 °C, which was significantly higher than the reported melting temperature of the A380 alloy (566±50 °C). Casting of the ingots was made in metallic gravity moulds, pre-heated at 500 °C. The moulds were placed on ceramic plates and were constantly vibrated at 200 Hz to ensure that any micro-bubbles entrapped in the melt during the casting process were removed and that the buoyancy of the fly-ash particles in the molten alloy would not tend to macro-differentiate the CFA content due to floating or sinking of the particles. After vibration at the above frequency level for about 3 minutes the mould was quenched in water and the ingots were removed and left to cool in air. No further thermal treatment for

the ingots (i.e. ageing or annealing) was applied. In total the following specimens were produced from casting.

The dimensions of each ingot were roughly 100×50×12 mm. All ingots width-wise were slightly less than 50mm in the middle due to shrinkage. The cast ingots were subsequently machined to produce a variety of specimens for different purposes (tests), namely tensile testing, compressive testing, Charpy impact testing, Brinell hardness testing, pin-on-disc friction testing and metallurgical characterisation. The details are given in Table 2.

Machining was carried out using uncoated carbide end-mills for face and side milling of the ingots. No cutting fluid was used during machining (dry machining) but the surfaces were cooled and the chips were removed using a continuous air jet. As expected, the cutting tools showed some mild signs of wear, particularly when machining the 10 wt% CFA samples.

4.3. Sample preparation

Following the design and calibration of the equipment and the powder milling and melt-mixing sub-processes discussed in sections 2 and 3, small batches were produced in the laboratory using various selected CFA compositions:

a. batches of five (5) A380-CFA MMC specimens for fine particles sizes 0, 1, 5, and 10 wt% (sample codes 00, F01, F05 and F10 respectively) and
b. batches of three (3) A380-CFA MMC specimens for ultra-fine (<0.5 μm, as explained in section 4.1) particle sizes 0, 1, 5, and 10 wt% (sample codes U01, U05 and U10 respectively).

The materials and produced specimens underwent experimental characterisation at various steps. These are presented and discussed in the following sections.

4.4. Mechanical testing experimental procedures

For the mechanical characterisation of the A380 castings the following laboratory equipment (testing machines) was used:

- INSTRON universal testing system, model 4482, ±100 kN, max velocity 500 mm/min, 1000mm stroke
- Hardness tester PROCEQ EQUO TIP2
- Friction tester (Pin-on-Disk) Anton Paar tribometer

The mechanical characterisation included tensile, compressive, impact, hardness and friction testing and was carried out as described in the following sections.

4.4.1. Tensile testing

Specimens were cut from the ingots at a length of 100mm, width 10mm, and thickness 6mm. From these, a central gauge area was machined measuring 25±0.1mm long by 6±0.1mm wide according to the relevant standard ASTM B557 M – 15 [38]. At the central area of the gauge length two KYOWA 0-90 strain gauge rosettes were bonded (one on each side) and connected to form a full Wheatstone bridge. The specimens were placed on the INSTRON 4482 testing machine and were loaded at constant strain rate up to failure. The maximum load and the yield load were recorded as well as the elongation at break.

4.4.2. Compressive testing

Cylindrical specimens were cut from the ingots measuring 13±0.2 mm in diameter and 20±1mm long according to the relevant standard ASTM E9 – 09 [39]. The specimens were placed on the universal testing machine and were loaded at constant strain rate in compression up to failure. The maximum load at failure (yield) was recorded.

4.4.3. Charpy impact testing and Brinell hardness testing

Prismatic specimens were cut from the ingots measuring 55x10x10mm in size and a 45° V-notch at 2mm depth was machined at their mid-span according to the relevant standard ASTM E23 - 16b [40]. The specimens were placed on the anvil of a standard Charpy V-notch impact testing machine as simply supported beams. The hammer was placed at 90° and was released to break the specimen. The angle of the hammer after impact was recorded and from the data the absorbed energy was calculated. On the same specimen one side was polished for metallurgical observations (material characterisation) prior to the Charpy testing and at an end Brinell hardness measurements were taken.

4.4.4. Friction and wear testing

Polished prismatic specimens were also used for friction and wear testing. Separate samples were used than the other tests, in order to avoid an ageing effects due to temperature build-up during the friction and wear testing. The samples were placed on the Pin-on-Disk tribometer and loaded with an equivalent compressive stress of 2 MPa. Due to the prior polishing of the surface, it was ensured that the hardened pin came in full contact with the metallic surface to be tested and the tribometer pin started to reciprocate with a sliding velocity of 0.25 m/min. The wear rate was measured directly from the instrument as change in the penetration depth (originally zero) over time and the test was ended when the total penetration reached 0.2 mm (200 µm). The measured wear rate (in µm/min) and the mean coefficient of sliding friction (f) were recorded.

5. Characterisation results and discussion

5.1. Metallurgical characterisation of the solidified castings

Two samples F05 and U05, each with 5 wt% CFA content, were prepared and polished with SiC paper for SEM study. Although no etching was performed on the specimens, the granular structure of the A380 alloy was clearly visible, with grains measuring roughly 100µm in size, which were clearly demarcated with Si-rich grain boundaries (Fig. 6a). Ground CFA particles were readily observed on the SEM images (Fig. 6b-c) and their identity was verified with EDS showing clear Ca and Fe lines on the obtained spectrum (Fig. 6d). Their size ranged from sub-micron to a few microns size as can be measured on the SEM images. No CFA agglomerates were observed, indicating very good de-agglomeration during the mixing phase. Also the CFA particles seem to be well-bonded with the surrounding Al matrix, with good interfacial strength, as no missing-particle cavities, which might have been created during polishing, were found on the specimen. The mixed CFA-A380 phase occupied an estimated 70% of the volume, reasonably well-dispersed across the specimen, with the balance being occupied by a pure A380 alloy phase. Presumably, this segregation took place during the solidification phase, facilitated by the finite cooling rate of the specimens.

5.2. Mechanical characterisation of samples

5.2.1. Tensile testing

The results are summarised in Figs. 9a-b, 10 and 11 (specimens 00, F01, F05, F10), also showing the scatter between the five specimens used for each material composition. It is confirmed that the use of increased fly-ash content raises the UTS and yield stress limits. Correspondingly, the elongation at failure is considerably decreased in all cases. The Young's modulus remained practically unaffected.

SEM micrographs of the fracture surface of one F01 specimen (Figs. 7a-b) and one U01 specimen (Fig. 7c) revealed that the crack propagated preferentially through the CFA-A380 patches. This is likely due to the local stiffening effect of the CFA, which causes the CFA-A380 patches to take on a higher load compared to the surrounding matrix material. The crack surface was mostly covered by 'cup-and-cone' features, which evidence a simultaneous development of multiple cracks of a predominantly ductile nature, which eventually joined to form the final crack surface. However, there were also locations where brittle fracture became dominant (Fig. 7b). At the bottom of several 'cups' CFA particles were identified, suggesting that these particles acted as crack initiators, presumably due to the stress concentration at the particle-matrix interfaces. Apart from the size of the visible CFA particles, the morphology of the crack surfaces in the F- and U-series samples was similar.

We therefore suggest the following mechanism to explain the mechanical behaviour of the CFA-A380 composite:

- The relatively evenly dispersed CFA particles, due to their good bonding with the A380 matrix, act as stiffening and reinforcing elements, increasing the strength and stiffness of the composite accordingly. The fine size and regular shape of the CFA particles causes a reduction of defects, compared to to larger particles, allowing a better utilisation of the Al-, Si- and Fe- oxides that together account for nearly 90 wt% of the CFA, as they become more resilient. The relatively even dispersion serves to reduce stress concentration within the composite.
- Due to the stress concentration, the interfaces of some CFA particles and the A380 matrix are starting locations for yielding. As some interfaces yield, the load is redistributed to neighbouring interfaces, which causes them to yield in turn, thus eventually leading to near simultaneous initiation of predominantly plastic failures, often originating at the CFA-matrix interfaces. Due to the fine CFA particle sizes and multitude of small cracks, the stress intensity at each of the developing cracks does not increase beyond the critical value, meaning that the mode of fracture remains mostly ductile. Only when the multiple cracks start to merge is the rate of the phenomenon increased, possibly culminating in a final brittle fracture stage.

5.2.2. Compressive testing

The maximum load at failure (yield) is plotted in Fig. 12a (specimens 00, F01, F05, F10). Above 5%wt CFA content the specimens exhibited predominantly brittle behaviour, which was associated with the development of cracks, a phenomenon that was clearly accompanied by a sudden drop in load. Again, as in tension, an increase of the compressive strength was observed with increasing %wt CFAs content.

5.2.3. Charpy impact testing and Brinell hardness testing

The results are given in Figs. 13 and 14a (specimens 00, F01, F05, F10). As expected, a considerable drop in the absorbed plastic work is observed, which can be directly linked to the marked reduction of the elongation at failure of the tensile test. On the contrary, the hardness increased quite significantly with increasing CFA content.

5.2.4. Friction and wear testing

The measured wear rate (in μm/min) and the mean coefficient of sliding friction (f) is given in Figs. 15 and 16 (specimens 00, F01, F05, F10). From these results a clear trend is observed, as both wear rate and friction coefficients decrease with increasing wt% CFA. This can be attributed to the increasing presence of hard oxides, such as aluminium oxide, which are present in the CFA, on the material surface. On the other hand, the increased content in iron oxide, which has generally poor tribological characteristics, is suspected to detrimentally affect the wear rate; however, there is not sufficient published data using different known CFA compositions to validate this hypothesis. Generally, CFA compositions with higher content in hard oxides can be expected to produce better results. A preliminary SEM study of the wear surface of one F01 sample was conducted, showing wear tracks and some CFA particles (Fig. 8), but EDS results did not show significant transfer of material, presumably due to the small particle size and low CFA content.

6. Effect of particle size

Additional test results were obtained from tension, compression and hardness testing as per the previously described protocols for the U01, U05 and U10 ('ultra-fine' particle) samples. Some of these are shown in Figs. 11c, 12b and 14b, where also the rolling average lines for the 00, F01, F05, F10 ('fine' particle) samples are plotted for reference (black lines). A clear increase in the UTS, the maximum compressive stress and the BHN can be seen compared to the reference. This confirms the hypothesis that finer CFA particle sizes lead to an improvement in the mechanical properties of CFA aluminium matrix alloys [12-13] and particularly in the case of A380 alloy.

Indeed, it follows from the model described in section 5.2.1 that finer CFA size distribution and dispersion will lead to same increase of stiffness and strength, according to the law of mixtures, and at the same time lower stress concentrations at the particle-matrix interfaces, and, when cracks do initiate, to a situation where the cracks sizes, stress intensities, and thus crack propagation rates will be relatively lower. This provides a theoretical underpinning to the experimental observations.

7. Conclusion

MMCs using ultra-fine CFA particles were produced using the castable aluminium alloy A380. In order to reduce the CFA particle size, a novel prototype ring-mill was used for efficient reduction of the particles to micron or submicron sizes (1 μm average), which are lower than all reported studies to date (4 μm average). The milling time (2 hrs) was also considerably reduced compared to conventional planetary ball milling (30 hrs). The produced CFA in the form of agglomerates was then mixed with the molten metallic matrix using a novel extensional flow melt-mixing device that provided deagglomeration and uniform dispersion of singular fly-ash particles within the melt. Castings from these MMCs with different %wt.

contents of pulverised ultra-fine CFA were produced and tested in a number of mechanical tests.

The metallurgical characterisation tests proved that the breakup of the agglomerates and the dispersion of the particles within the metallic matrix was complete and, as expected, the wt% increase in CFA led to an increase in strength, hardness and wear resistance, but at the cost of ductility and toughness. The mechanical tests further showed that for the same wt% CFA content, the finer CFA particle sizes led to an improvement of the mechanical properties, confirming earlier observations by Anilkumar [12] performed with much coarser particle sizes. This last finding suggests that further effort is warranted to minimise average particle sizes to sub-micron range by further improving the introduced CFA ring-milling process.

Acknowledgements

This work was supported by the internal fund for research of Nazarbayev University (project NANOCAST, grant No. SOE2016002) and the Ministry of Education and Science of Kazakhstan. The authors would also like to thank the thermal power plants of Oskemen and Astana cities for generously providing with CFA samples to carry out the studies.

References

1. Doel, T.J.A. and Bowen, P., 1996. Tensile properties of particulate-reinforced metal matrix composites. Composites Part A: Applied Science and Manufacturing, 27(8), pp.655-665.
2. Prasad, SV and Asthana, R, 2004. Aluminum metal-matrix composites for automotive applications: tribological considerations. Tribology letters 17 (3), pp. 445-453
3. Karantzalis, A. E., Lekatou, A., Georgatis, E., Poulas, V., & Mavros, H. (2010). Microstructural observations in a cast Al-Si-Cu/TiC composite. Journal of Materials Engineering and Performance, 19(4), 585-590.
4. Rohatgi, PK, 1994. Low-cost, fly-ash-containing aluminum-matrix composites. JOM - Journal of the Minerals, Metals and Materials Society 46 (11), 55-59
5. Rohatgi, PK, Guo RQ, Iksan, H, Borchelt, EJ, Asthana, R, 1998. Pressure infiltration technique for synthesis of aluminum–fly ash particulate composite. Materials Science and Engineering: A 244 (1), 22-30
6. Yang, Y., Lan, J. and Li, X., 2004. Study on bulk aluminum matrix nano-composite fabricated by ultrasonic dispersion of nano-sized SiC particles in molten aluminum alloy. Materials Science and Engineering: A, 380(1), pp.378-383.
7. Gikunoo, E., Omotoso, O. and Oguocha, I.N.A., 2005. Effect of fly ash particles on the mechanical properties of aluminium casting alloy A535. Materials science and technology, 21(2), pp.143-152.
8. Surappa, M.K., 2008. Synthesis of fly ash particle reinforced A356 Al composites and their characterization. Materials Science and Engineering: A, 480(1), pp.117-124.
9. Moutsatsou, A., Itskos, G., Vounatsos, P., Koukouzas, N., Vasilatos, C. Microstructural characterization of PM-Al and PM-Al/Si composites reinforced with lignite fly ash. Materials Science and Engineering: A 527 (18), 4788-4795.
10. Zahi S., Daud A.R. (2011) Fly ash characterization and application in Al-based Mg alloys. Materials and Design 32 (3) pp. 1337-1346
11. Itskos, G., Moutsatsou, A., Rohatgi, P.K., Koukouzas, N., Vasilatos C., Katsika E., 2011 Compaction of high-Ca fly ash-Al-and Al-alloy-composites: Evaluation of their microstructure and tribological performance. Coal Combustion and Gasification Products 3, 75-82.

12. Anilkumar, H.C., Hebbar, H.S. and Ravishankar, K.S., 2011. Mechanical Properties of Fly Ash Reinforced Aluminium Alloy (Al6061) Composites. International journal of mechanical and materials engineering, 6(1), pp.41-45.
13. Murthy, I.N., Rao, D.V. and Rao, J.B., 2012. Microstructure and mechanical properties of aluminum–fly ash nano composites made by ultrasonic method. Materials & Design, 35, pp.55-65.
14. Sahin, Y., 2003. Preparation and some properties of SiC particle reinforced aluminium alloy composites. Materials & design, 24(8), pp.671-679.
15. Ahlatci, H., Kocer, T., Candan, E. and Çimenoğlu, H., 2006. Wear behaviour of Al/(Al 2 O 3p+ SiC p) hybrid composites. Tribology international, 39(3), pp.213-220.
16. [16] Wu, S.Q., Wang, H.Z. and Tjong, S.C., 1996. Mechanical and wear behavior of an Al/Si alloy metal-matrix composite reinforced with aluminosilicate fiber. Composites science and technology, 56(11), pp.1261-1270.
17. Chawla, N., 2006. Chawla. KK,"Metal Matrix Composites". New York: Springer.
18. Ünlü, B.S., 2008. Investigation of tribological and mechanical properties Al 2 O 3–SiC reinforced Al composites manufactured by casting or P/M method. Materials & Design, 29(10), pp.2002-2008.
19. Kumar, G.V., Rao, C.S.P. and Selvaraj, N., 2012. Studies on mechanical and dry sliding wear of Al6061–SiC composites. Composites Part B: Engineering, 43(3), pp.1185-1191.
20. Wahab, M.N., Daud, A.R. and Ghazali, M.J., 1970. Preparation and characterization of stir cast-aluminum nitride reinforced aluminum metal matrix composites. International Journal of Mechanical and Materials Engineering, 4(2).
21. Basavarajappa, S., Chandramohan, G. and Dinesh, A., 2004, December. Mechanical properties of mmc's-An experimental investigation. In Int. symposium of research on Materials and Engineering, IIT, Madras, December (Vol. 20, pp. 1-8).
22. Jiang, W., Fan, Z., Li, G., Yang, L., & Liu, X. (2016). Effects of melt-to-solid insert volume ratio on the microstructures and mechanical properties of Al/Mg bimetallic castings produced by lost foam casting. Metallurgical and Materials Transactions A, 47(12), 6487-6497.
23. Jiang, W., Li, G., Fan, Z., Wang, L., & Liu, F. (2016). Investigation on the interface characteristics of Al/Mg bimetallic castings processed by lost foam casting. Metallurgical and Materials Transactions A, 47(5), 2462-2470.
24. Charles, S. and Arunachalam, V.P., 2004. Property analysis and mathematical modeling of machining properties of aluminium alloy hybrid (Al-alloy/SiC/flyash) composites produced by liquid metallurgy and powder metallurgy techniques.
25. Mahendra, K.V. and Radhakrishna, K., 2007. Fabrication of Al-4.5% Cu alloy with fly ash metal matrix composites and its characterization. Materials Science-Poland, 25(1), pp.57-68.
26. Sudarshan, S., MK 2008. Synthesis of fly ash particle reinforced A356 Al composites and their characterization. Material Science and Engineering, A, 480, pp.117-124.
27. Itskos, G., Rohatgi, P.K., Moutsatsou, A. DeFouw, J.D., Koukouzas, N., Vasilatos, C., Schultz B.F., 2012. Synthesis of A356 Al–high-Ca fly ash composites by pressure infiltration technique and their characterization. Journal of Materials Science 47 (9), 4042-4052.
28. Rohatgi, P.K., Daoud, A., Schultz, B.F. and Puri, T., 2009. Microstructure and mechanical behavior of die casting AZ91D-Fly ash cenosphere composites. Composites Part A: Applied Science and Manufacturing, 40(6), pp.883-896.
29. Spitas, V., & Spitas, C. (2012). Stochastic simulation of the power requirements of dry clinker pulverisation. International Journal of Mineral Processing, 106, 42-49.

30. Spitas, V., Makris, P. and Founti, M., 1999. A novel dry pulverizer for low cost production of powders. Particulate science and technology, 17(3), pp.217-228.
31. West, R.D. and Malhotra, V.M., 2006. Rupture of nanoparticle agglomerates and formulation of Al2O3-epoxy nanocomposites using ultrasonic cavitation approach: Effects on the structural and mechanical properties. Polymer Engineering & Science, 46(4), pp.426-430.
32. Kaisarlis, G., Tsolakis, E., Vasileiou, G., Spitas, V., Tauanov, Z., Inglezakis, V., ... & Spitas, C. (2018). Efficient oscillating micro-grid mixing of CFA-aluminium composite melts. Journal of Materials Processing Technology, 254, 60-71.
33. Tauanov, T., Abylgazina, L., Nurmukhambetov, D., Baimenov, A., Spitas, C. Itskos, G. and Inglezakis, V.J., 2017. Mineralogical, microstructural and thermal characterization of coal fly ash produced from kazakhstani power plants. 2017 International Conference on Materials Sciences and Nanomaterials (ICMSN 2017), July 14-16, 2017 Barcelona, Spain
34. Querol, X., Moreno, N., Umaña, J.T., Alastuey, A., Hernández, E., Lopez-Soler, A. and Plana, F., 2002. Synthesis of zeolites from coal fly ash: an overview. International Journal of coal geology, 50(1), pp.413-423.
35. Cardoso, A.M., Paprocki, A., Ferret, L.S., Azevedo, C.M. and Pires, M., 2015. Synthesis of zeolite Na-P1 under mild conditions using Brazilian coal fly ash and its application in wastewater treatment. Fuel, 139, pp.59-67.
36. Aldahri, T., Behin, J., Kazemian, H. and Rohani, S., 2016. Synthesis of zeolite Na-P from coal fly ash by thermo-sonochemical treatment. Fuel, 182, pp.494-501.
37. Ojumu, T.V., Du Plessis, P.W. and Petrik, L.F., 2016. Synthesis of zeolite A from coal fly ash using ultrasonic treatment–A replacement for fusion step. Ultrasonics sonochemistry, 31, pp.342-349.
38. ASTM B557 M – 15: Standard Test Methods for Tension Testing Wrought and Cast Aluminium- and Magnesium-Alloy Products
39. ASTM E9 – 09: Standard Test Methods of Compression Testing of Metallic Materials at Room Temperature
40. ASTM E23 – 16b: Standard Test Methods for Notched Bar Impact Testing of Metallic Materials

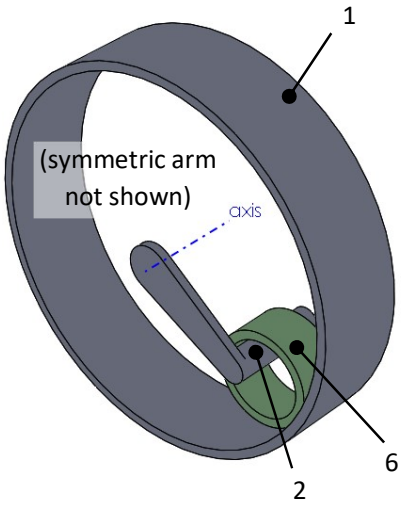
1
(symmetric arm
not shown)
axis
2
6

(a)

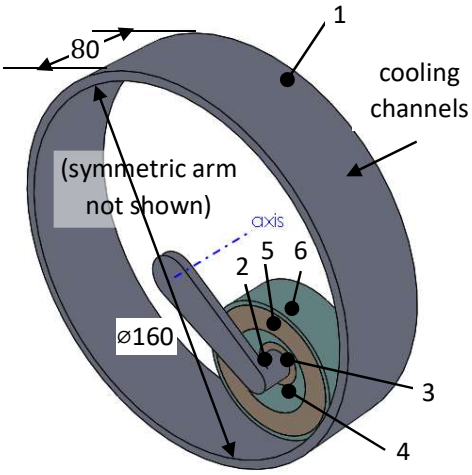
80
1
cooling
channels
(symmetric arm
not shown)
axis
2
5
6
⌀160
3
4

(b)

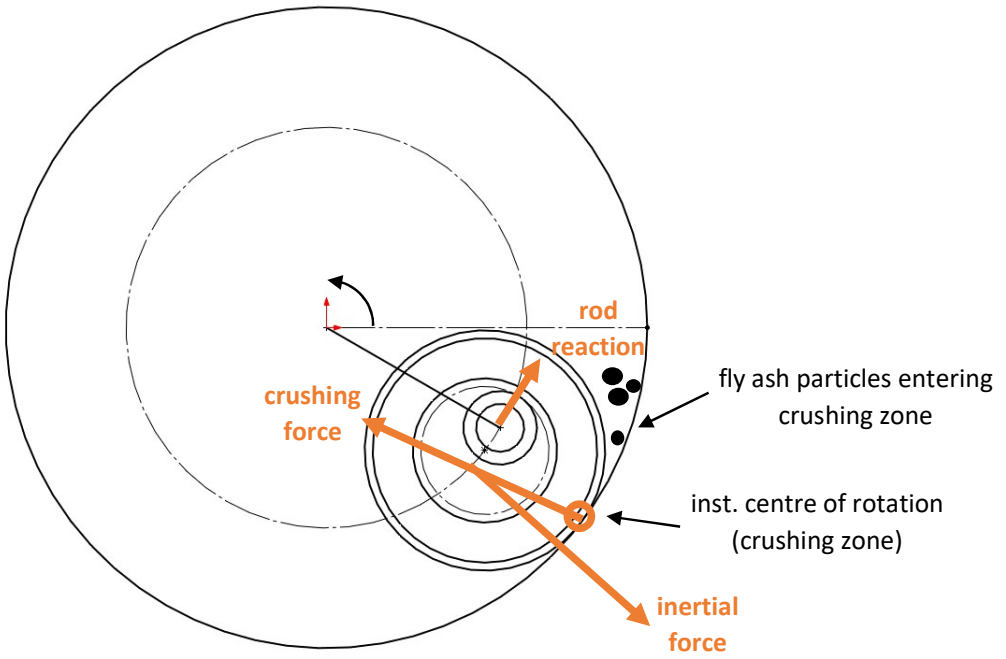

(c)

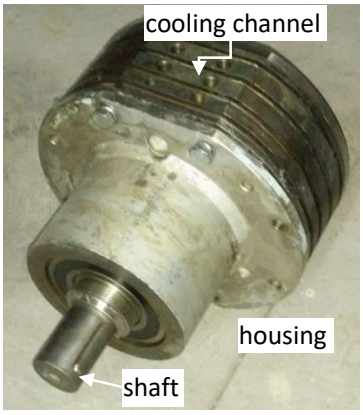

(d)

Fig. 1: Construction of the ring-mill, showing a slice of the apparatus containing a single ring (only half of the rotating frame is shown for simplicity) –figure not to scale. a) Conventional ring mill; b) Improved ring mill with bearing, used in this study; c) Operating principle of improved ring mill (only one ring shown); d) Photograph of ring mill pulveriser body with cooling channels

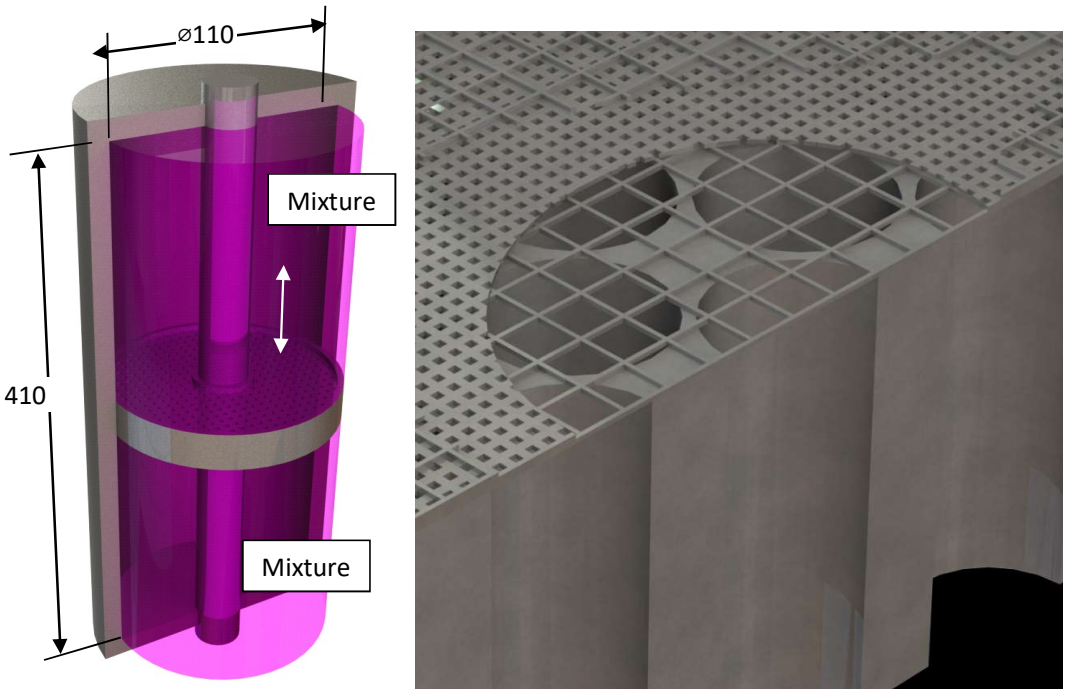

(a) (b)

Fig. 2: The oscillating micro-grid melt-mixing apparatus. a) Mixing cavity, showing half of the cylinder, and the piston, including its grid (simplified); b) Detail of the grid and supporting structure.

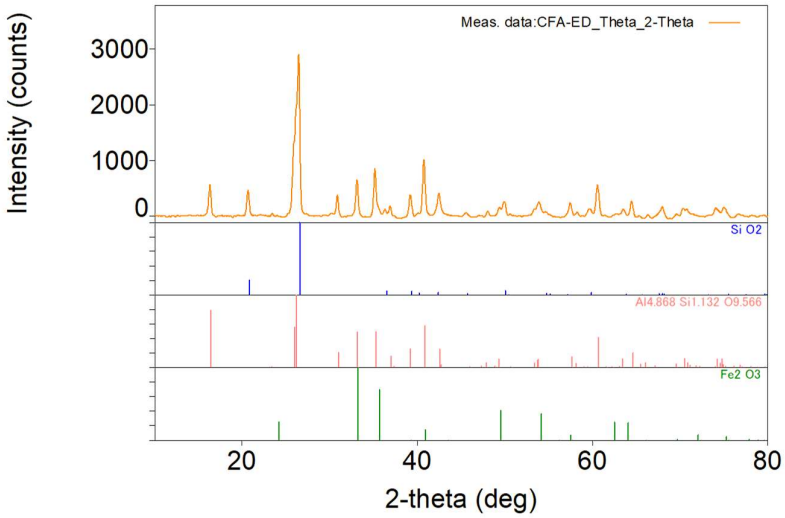

Fig. 3: XRD spectrum of the CFA batch

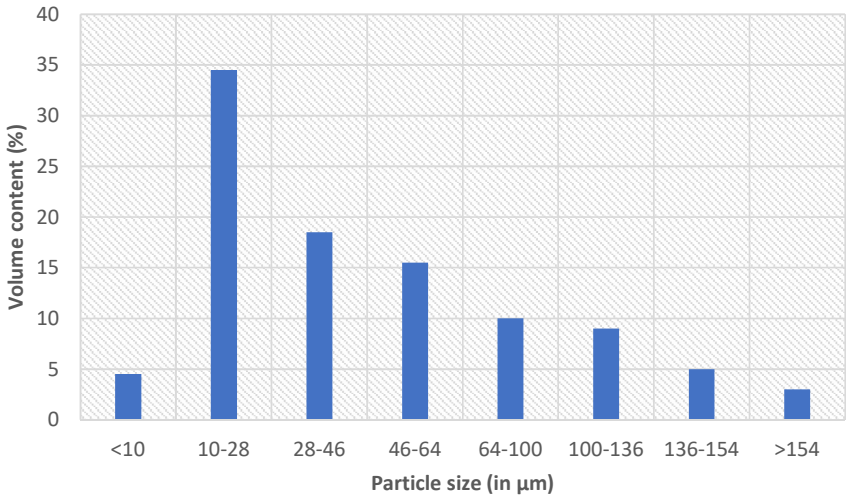

(a)

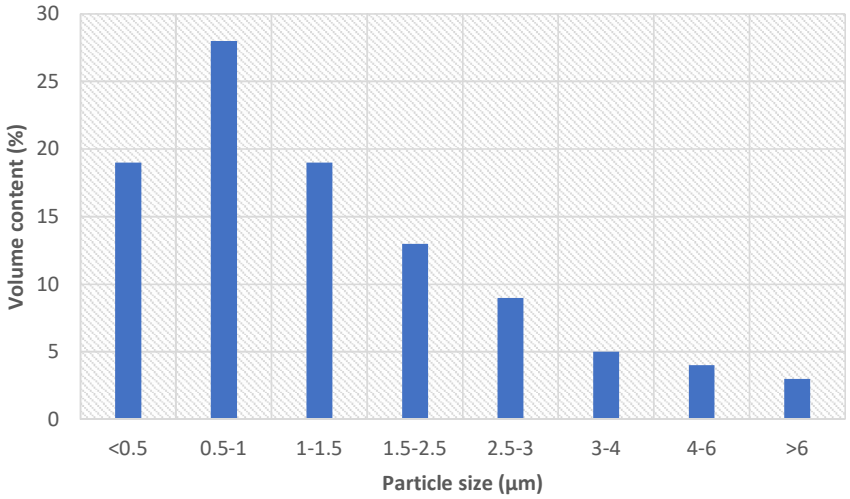

(b)

Fig. 4: CFA particle size distribution. a) Original; b) Pulverised after 120 min in the high performance ring mill.

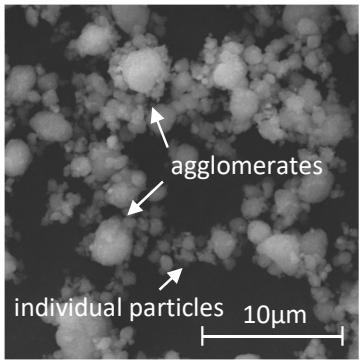

Fig. 5: SEM micrograph of the milled CFA, showing various particle sizes and agglomerates

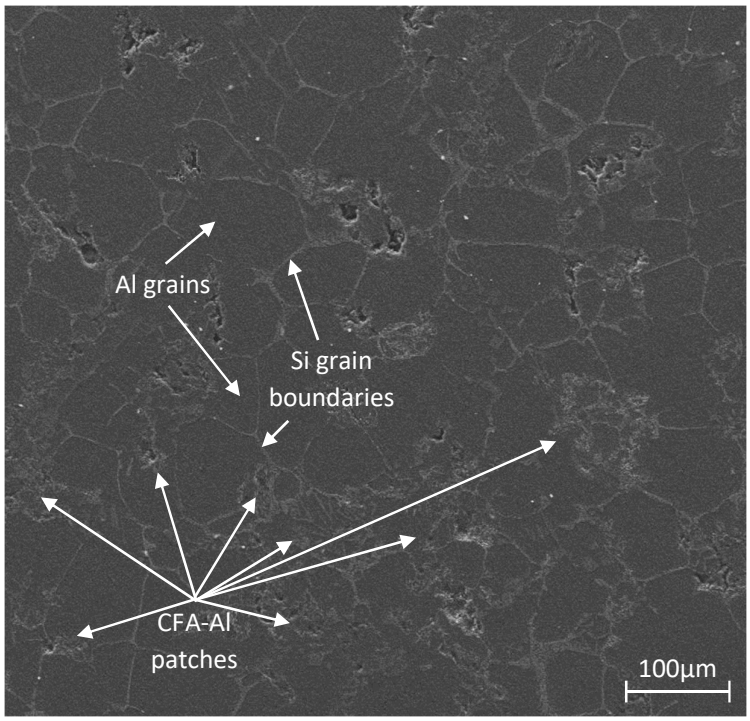
Al grains
Si grain boundaries
CFA-Al patches
100µm

(a)

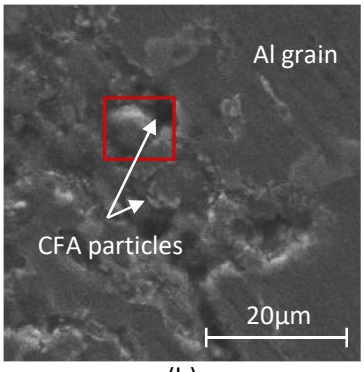
Al grain
CFA particles
20µm

(b)

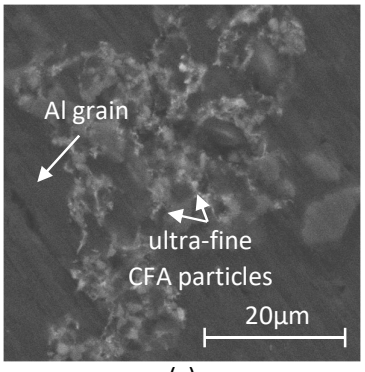
Al grain
ultra-fine CFA particles
20µm

(c)

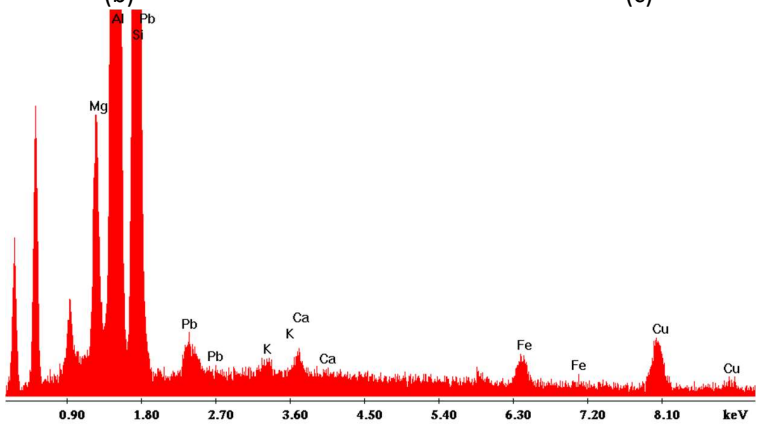
Al
Pb
Si
Mg
Pb
Pb
K
Ca
K
Ca
Fe
Fe
Cu
Cu
0.90
1.80
2.70
3.60
4.50
5.40
6.30
7.20
8.10
keV

(d)

Fig. 6: SEM micrographs of CFA-A380 composite, 5 wt% CFA, polished. a-b) Sample F05, showing an approx. well-mixed CFA-aluminium phase, occupying an estimated 70% of the total volume, the balance being a standard aluminium grain structure. The CFA nanoparticles resisted the polishing and are discernible as lumps. Adjoining Al grains can also be seen; c) Sample U05, characterised by finer CFA particles; d) EDS analysis of sample (a) –area marked by red rectangle, confirming the presence of CFA (Ca, Fe).

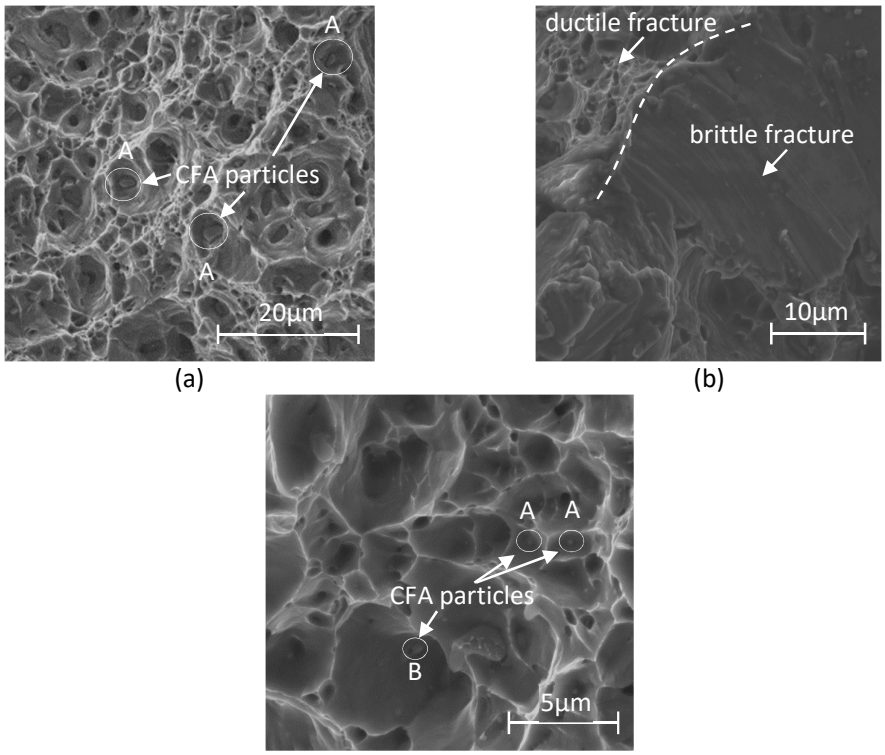

Fig. 7: SEM micrographs of fracture surface of CFA-A380 composite, 1 wt% CFA. Multiple adjacent cup-and-cone formations, often with CFA particles visible at their bottom/ origin. Isolated particles at the bottom of the 'cup' formations (marked A) are likely crack initiation sites, whereas some other visible particles (marked B) do not seem to have affected crack propagation. a-b) Sample F01, showing both ductile and brittle fracture regions; c) Sample U01, showing similar morphology but with only ultra-fine particles.

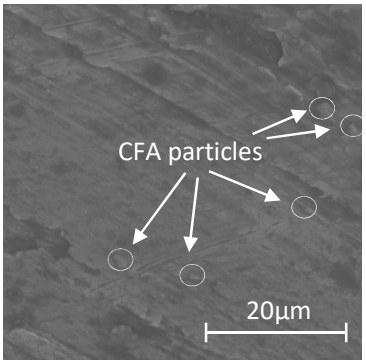

Fig. 8: SEM micrograph of worn surface (pin-on-disc) of CFA-A380 composite, sample F01. Some CFA particles are visible. Wear marks can be seen along the direction of sliding.

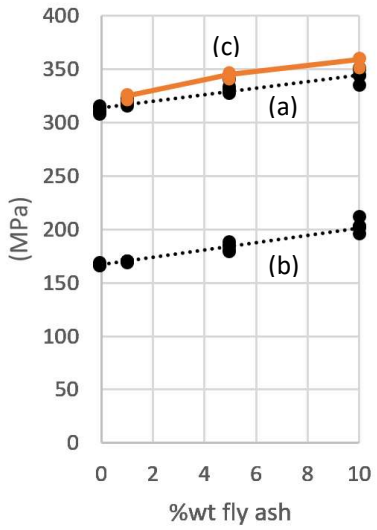

Fig. 9: a) Ultimate tensile stress, F-series; b) Yield stress, F-series and c) Ultimate tensile stress, U-series vs. CFA content

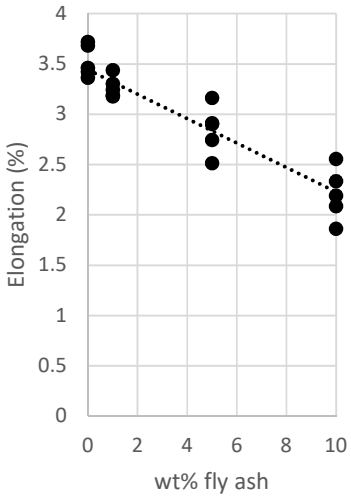

Fig. 10: Elongation vs. CFA content

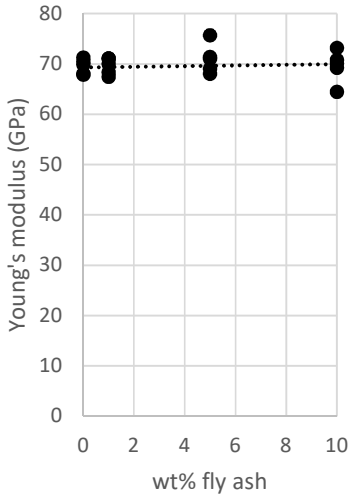

Fig. 11: Young's modulus vs. CFA content

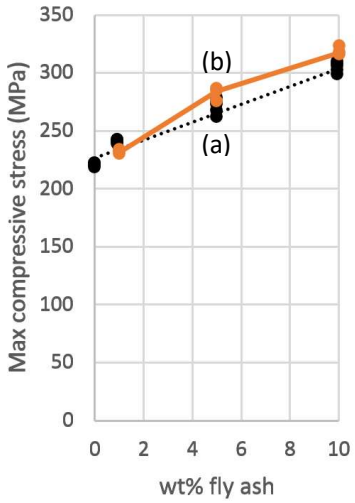

Fig. 12: Maximum compressive stress vs. CFA content. a) F-series, b) U-series.

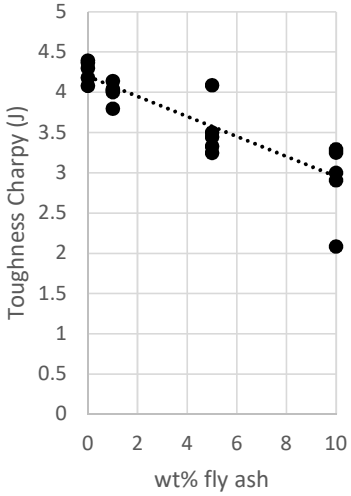

Fig. 13: Charpy toughness vs. CFA content

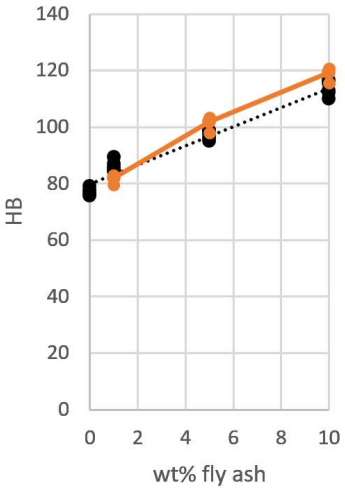

Fig. 14: Brinell hardness vs. CFA content. a) F-series, b) U-series

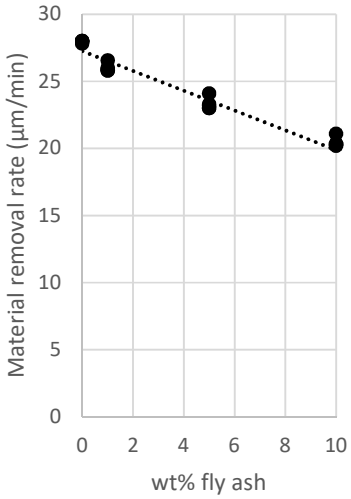

Fig. 15: Material removal rate vs. CFA content (pin on disc)

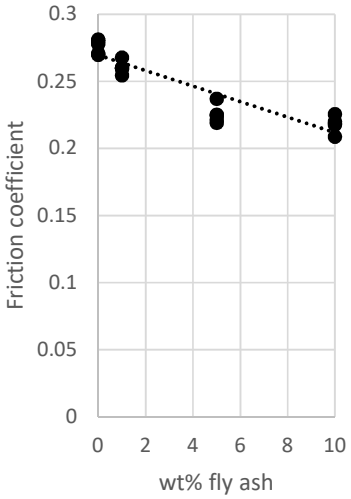

Fig. 16: Sliding friction coefficient vs. CFA content (pin on disc)

Table 1: Elemental composition of the CFA batch used in this study

Compound	%wt
Na_2O	0.187
MgO	0.628
Al_2O_3	18.071
SiO_2	44.128
SO_3	0.204
Cl	0.138
K_2O	0.514
CaO	6.077
TiO_2	1.353
Cr_2O_3	0.035
MnO	0.608
Fe_2O_3	27.786
CuO	0.032
ZnO	0.013
Ga_2O_3	0.008
SrO	0.059
Y_2O_3	0.008
ZrO_2	0.048
BaO	0.103

Table 2: Composition of A380 alloy used for casting

Al	Cu	Mg	Fe	Sn	Ni	Zn	Mg	Si	other
Bal.	3.0-4.0	0.1	<1.3	<0.35	<0.5	3.0	0.5	7.5-9.5	0.5